IRSTI 29.19.22; 47.09.48 https://doi.org/10.26577/ijmph.20261714

AMMONIA SENSING PROPERTIES OF FLUORINATED Si@C CORE–SHELL HYBRIDS

D. Yermukhamed[1,2], S.Z. Baktygerey[2], G.Sh. Yar-Mukhamedova[2], A.M. Serikbekov[2], O.Yu. Boldyrieva[3], V. Lysenko[4], V.V. Lisnyak[5] and G.K. Mussabek[1,2]

[1] *Institute of Information and Computational Technologies, Almaty, Kazakhstan*
[2] *Al-Farabi Kazakh National University, Almaty, Kazakhstan*
[3] *Chemical Faculty, Kyiv National Taras Shevchenko University, Kyiv, Ukraine*
[4] *Light Matter Institute, UMR-5306, Claude Bernard University of Lyon, Villeurbanne, France*
[5] *Institute of Surface Chemistry, NAS of Ukraine, Kyiv, Ukraine*

Email: danayermukhamed92@gmail.com

(Received 4 April 2026; revised 27 April 2026; accepted 12 May 2026)

Abstract. Silicon nanoparticles encapsulated in carbon shells (Si@C) were synthesized via polymer-derived carbonization and subsequently fluorinated by gas-phase treatment to tailor their interfacial electronic properties. The resulting Si@C–F core–shell nanostructures were investigated as chemiresistive sensors for ammonia detection at room temperature. The fluorinated hybrids exhibit a 2–2.5-fold enhancement in response toward NH_3 in the 1–20 ppm range, while maintaining linear behavior (R^2>0.99) at low concentrations. The enhanced performance is attributed to fluorination-induced modulation of interfacial electronic states and the barrier height at the Si/SiO_x/C:F heterojunction. The introduction of electron-withdrawing C–F groups increases the work function of the carbon shell and strengthens interfacial dipole fields, leading to amplified resistance modulation under NH_3 adsorption. Owing to the nanoscale dimensions of the silicon cores (20-40 nm), comparable to the Debye length, surface charge variations significantly influence charge transport. The sensors demonstrate high selectivity toward ammonia over alcohol vapors (ppm-normalized selectivity >10^4) and stable operation under moderate humidity. These findings establish fluorination as an effective strategy for engineering interfacial charge transfer in Si–C hybrids for room-temperature gas sensing.

Keywords: Si@C hybrids; fluorinated carbon; ammonia sensing; core–shell nanostructures; chemiresistive gas sensor.

INTRODUCTION

Semiconductor gas sensors remain among the most widely employed platforms for the detection of toxic, flammable, and environmentally hazardous gases, owing to their structural simplicity, cost-effectiveness, and compatibility with microelectronic fabrication technologies. Their operating principle is based on the modulation of electrical conductivity induced by adsorption–desorption processes at the semiconductor surface. Interactions between gas molecules and surface electronic states lead to charge transfer, which alters the width of the space-charge region and, consequently, the electrical resistance of the sensing layer. In nanoscale semiconductors, this effect is particularly pronounced, as the Debye length becomes comparable to the particle size; thus, even minor variations in surface charge density can significantly influence bulk conductivity [1, 2]. Silicon nanostructures have been extensively investigated for electronic and sensing applications due to their tunable electrical properties and inherent compatibility with semiconductor device architectures. In particular, porous silicon and silicon nanoparticles have attracted considerable attention because of their high specific surface area, adjustable conductivity, and the presence of native oxide layers (SiO_x) that serve as adsorption-active sites. However, silicon-based sensors often suffer from limitations such as the relatively low intrinsic conductivity of partially oxidized nanosilicon, instability of the surface oxide layer, insufficient selectivity toward target gases, and weak signal modulation under room-temperature conditions [3, 4].

Hybridization with carbon nanostructures has emerged as an effective strategy to overcome these challenges. The incorporation of car-

bon coatings enhances structural stability and facilitates charge transport across heterointerfaces, while carbon nanomaterials themselves offer high electrical conductivity, chemical robustness, and tunable surface chemistry [4, 5, 6]. Previous studies have demonstrated that carbon species, including graphene and carbon nanotubes integrated with silicon, can significantly influence sensor performance by modifying local electric fields, interface states, and defect-mediated recombination processes [7]. In Si@C systems, the formation of a Si/SiO_x/C heterointerface leads to band bending and charge redistribution driven by differences in work function, thereby improving sensing characteristics [8, 9, 10]. Nevertheless, pristine carbon coatings typically exhibit limited selectivity and relatively weak interactions with polar gas molecules, necessitating targeted chemical functionalization.

Fluorination of carbon materials represents a particularly promising approach to tailoring interfacial electronic properties. The incorporation of electron-withdrawing – CF_x groups increases surface polarity and modifies band alignment by withdrawing electron density from the π -electron system, thereby generating electron-deficient carbon centers and increasing the work function of the carbon phase [11, 12]. When fluorinated carbon shells are integrated with silicon nanoparticles, significant modifications of the interfacial electronic structure are expected. In particular, increased work function and the formation of interfacial dipoles can alter band bending and modulate the effective barrier height at the Si/SiO_x/C:F junction, enhancing sensitivity to surface charge perturbations. Since work-function variation directly governs barrier height and depletion width in gas-sensing systems, such modifications are critical for performance optimization [13].

Furthermore, fluorination can induce internal electric fields associated with C–F dipoles, increasing the responsiveness of the depletion layer to adsorption-induced charge transfer. It may also introduce structural disorder and edge defects that enhance the adsorption of electron-donating gases such as ammonia [14]. In this context, electron transfer from NH_3 to electron-deficient fluorinated carbon is expected to induce pronounced modulation of carrier concentration within the silicon core. Consistent with this mechanism, enhanced ammonia sensitivity has been reported for fluorinated graphene-based systems [15]. Accordingly, the sensing mechanism in fluorinated Si@C nanohybrids can be understood as a coupled process involving (i) gas adsorption on the C:F surface, (ii) charge transfer through the carbon shell, and (iii) modulation of the depletion layer within the silicon nanoparticle. The Si/SiO_x/C:F heterointerface thus acts as a tunable nanojunction, where fluorination governs surface polarity, band alignment, interfacial electric fields, and, ultimately, sensor response. On this basis, the present study investigates the room-temperature ammonia sensing performance of fluorinated Si@C core–shell nanostructures, with particular emphasis on the role of interfacial electronic structure in determining sensor behavior.

Despite extensive studies on Si–C hybrid systems, the role of fluorination in tuning interfacial electronic structure and its impact on room-temperature gas sensing remains insufficiently explored. In particular, the effect of fluorination-induced dipoles and work-function modulation on barrier-controlled transport has not been systematically addressed. This study aims to fill this gap by investigating fluorinated Si@C core–shell nanostructures as model nanoheterojunctions for ammonia sensing.

The novelty of this work lies in the use of fluorination as a tool to modulate interfacial electronic structure in Si@C hybrids, enabling enhanced barrier sensitivity and improved room-temperature ammonia detection.

EXPERIMENTAL

Materials

Powdered silumin alloy (80 wt.% Al-20 wt.% Si) was used as the silicon precursor. Hydrochloric acid (HCl, 15%), polyvinylpyrrolidone (PVP, average molecular weight $\approx$ 40,000), absolute ethanol, and analytical-grade ammo-

nia solution were used without further purification. Methanol and ethanol ($\geq$ 99.5%) were employed as interfering vapors. High-purity argon (99.999%) served as both carrier and protective gas.

Preparation of Silicon Nanoparticles

Si NPs were synthesized via selective acid etching of powdered silumin alloy [16]. The alloy powder was immersed in 15 wt.% aqueous HCl under continuous magnetic stirring for 8 h at room temperature to remove aluminum. The resulting solid residue was collected by filtration and thoroughly washed with deionized water until neutral pH was achieved. The obtained silicon nanopowder was subsequently dried in air at 120 °C for 12 h.

Preparation of Si@C Hybrid Nanostructures

For carbon coating, 100 mg of silicon nanopowder was dispersed in 100 mL of absolute ethanol containing 1 g of polyvinylpyrrolidone (PVP). The suspension was subjected to combined magnetic stirring and ultrasonication (20 kHz) for 30 min to ensure homogeneous adsorption of the polymer precursor onto the Si NP surface. The solvent was then removed using a rotary evaporator at 35 °C. The resulting solid was dried at 75 °C for 12 h.

Carbonization was carried out in a fluidized-bed furnace under a continuous argon flow (100 mL·min^{-1}) at 400 °C for 4 h, with a heating rate of 5 °C·min^{-1}. The obtained Si@C nanohybrids consist of crystalline silicon cores (20–40 nm) encapsulated by semi-amorphous carbon shells with a thickness of approximately 0.5–2 nm.

Fluorination of Carbon Shell

Fluorination of the carbon shell was performed via gas-phase treatment [17, 18]. Typically, 1–5 g of Si@C powder were placed in a quartz tubular reactor, heated to 400 °C, and exposed for 2 h to a flowing gas mixture containing 50 vol% 1,1,1,2-tetrafluoroethane ($C_2H_2F_4$) diluted in argon. The total gas flow rate was maintained at 100 mL·min^{-1}. Following fluorination, the samples were purged and cooled to room temperature under a dynamic argon atmosphere to prevent oxidation. The resulting Si@C–F nanohybrids are expected to contain surface functional groups such as C–F, CF_2, and CF_3 [18]. The powders were subsequently washed with deionized water and dried to remove residual byproducts.

Structural and Morphological Characterization

Morphological analysis was conducted using scanning electron microscopy (SEM, Tescan Mira 3) at an accelerating voltage of 15 kV. Transmission electron microscopy (TEM) investigations were performed on a JEOL JEM-3000F microscope operating at 200 kV. For fluorinated samples, energy-dispersive X-ray (EDX) spectroscopy was employed to confirm the presence and distribution of fluorine.

Sensor Fabrication

For gas-sensing measurements, the prepared nanopowders were deposited onto interdigitated electrode substrates by drop-casting from ethanol suspension. The deposited films were dried at 80 °C for 1 h to ensure adhesion. The resistance of the sensing layer was monitored using a digital multimeter under a constant applied voltage bias.

Gas Sensing Measurements

Gas-sensing experiments were carried out in a custom-built chamber operating at room temperature (25 ± 2 °C). High-purity argon was used as the carrier gas. Ammonia was introduced from a certified NH_3/Ar gas mixture and diluted to the desired concentrations (1–20 ppm) using calibrated mass flow controllers. For selectivity studies, methanol (CH_3OH, p.a.) and ethanol (C_2H_5OH, p.a.) vapors were generated under identical flow conditions and diluted to nominal concentrations of approximately 1000 ppm using calibrated mass flow controllers. Relative humidity (RH) was controlled by passing argon gas through a gas bubbler with water, while RH values were continuously monitored using a cal-

ibrated RS41 humidity sensor positioned inside the chamber. The sensor response (S) in relative units (r.u.) was defined as::

$$S = \frac{R_{\text{gas}} - R_0}{R_0} \quad (1)$$

where R_0 is the baseline resistance in pure argon, and R_{gas} is the resistance under analyte exposure. All measurements were performed with a sampling interval of 1 s [16].

Results and Discussion

High-Resolution TEM Analysis

Figure 1 presents high-resolution transmission electron microscopy (HRTEM) images of the pristine Si@C hybrid (Fig. 1a) and of the fluorinated Si@C–F hybrid (Fig. 1b). In both cases, the nanoparticles exhibit a well-defined core–shell architecture comprising a crystalline silicon core encapsulated by a thin carbon-derived shell. In Fig. 1a, the central region appears as a high-contrast domain characteristic of crystalline silicon. Although lattice fringes are not uniformly resolved across the entire particle, likely due to orientation and thickness variations, the observed contrast and texture are consistent with nanoscale crystalline Si. At the particle periphery, a thin, lower-contrast rim is clearly visible and is attributed to the carbon shell. Its morphology corresponds to a semi-amorphous carbon layer formed via PVP carbonization at 400 °C under an argon atmosphere. The interface between the Si core and the carbon shell appears diffuse, which is typical for silicon nanoparticles and can be ascribed to the presence of an ultrathin SiO_x interlayer (native oxide and oxygen-containing surface species formed during post-synthesis processing). Overall, the pristine Si@C hybrid consists of a crystalline Si core surrounded by a continuous, conformal semi-amorphous carbon shell with an estimated thickness of ~0.5–2 nm. This configuration establishes an extended Si/SiO_x/C heterointerface, which is expected to play a key role in governing charge transfer processes and sensor response.

In Fig. 1b, corresponding to the fluorinated Si@C–F hybrid, the silicon core remains structurally intact, with lattice fringes more clearly resolved in localized regions (as indicated in the annotated image), confirming that fluorination at 400 °C for 2 h does not disrupt the crystalline Si phase. The outer shell remains thin and conformal; however, it exhibits increased contrast heterogeneity and structural disorder relative to the pristine sample. This behavior is consistent with fluorination-induced modification of the carbon network [18], including the formation of C–F, CF_2, and CF_3 functional groups, an increased density of sp^3-like defects, and partial disruption of π-conjugation and turbostratic ordering. Importantly, fluorination preserves the overall core–shell morphology while primarily modifying the surface chemistry and electronic structure of the carbon shell. The incorporation of polar C–F functionalities [14, 15] and defect sites is expected to increase dipole density and alter the work function of the carbon phase, thereby enhancing interfacial barrier modulation under NH_3 adsorption.

Composition estimates and fluorine loading

Based on carbonization mass balance and surface-sensitive EDX analysis, the Si@C hybrid is estimated to comprise approximately 33–50 wt.% crystalline silicon cores and 50–67 wt.% carbonaceous shell. This distribution is consistent with the carbonization yield of PVP and the expected core–shell geometry. Following fluorination, the bulk fluorine content is determined as 0.20 mmol g^{-1} ($\approx$ 0.38 wt.%), where the uncertainty reflects calibration error and signal variability in EDX quantification (±10–15% relative) Surface-sensitive EDX measurements indicate that the carbon shell contains approximately 0.4 wt.% fluorine along with ~5 wt.% oxygen, the latter attributed to residual oxygen-containing surface functionalities and partial oxidation during post-treatment handling.

For spherical silicon cores of diameter d = 20 – 40 nm coated by a carbon shell of thickness t = 0.5 – 2 nm, the geometrical shell volume fraction can be estimated as:

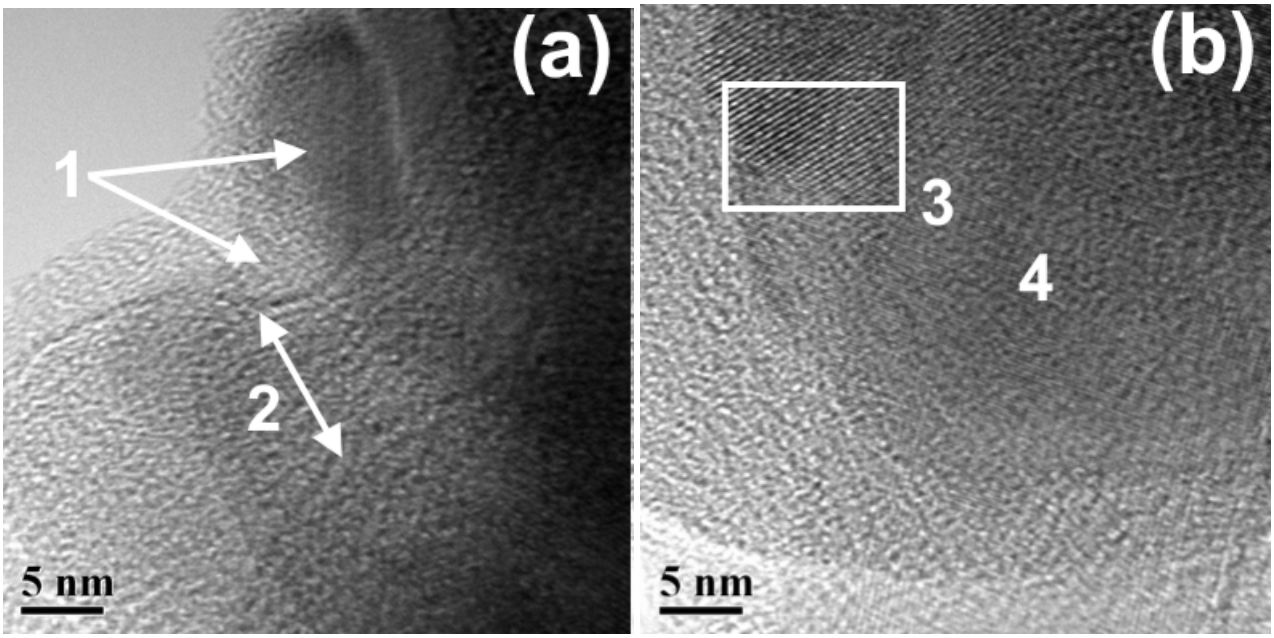

Figure 1 - HRTEM images of (a) pristine Si@C hybrid nanoparticles and (b) fluorinated Si@C–F nanoparticles. In (a), (1) a thin carbon-derived shell surrounding the Si core and (2) an ultra-thin interfacial SiO_x layer are indicated. In (b), (3) well-resolved lattice fringes corresponding to crystalline Si and (4) fluorination-induced structural disorder within the carbon shell are highlighted. Both materials exhibit a core–shell architecture with crystalline Si cores and a Si/SiO_x/C heterointerface. Fluorination preserves the crystalline Si lattice (3) while increasing structural disorder in the carbon shell (4), consistent with C–F bond formation and partial disruption of sp^2 domains.

$$f_{shell} = 1 - \left(\frac{d}{d+2t}\right)^3 \tag{2}$$

yielding d_{shell} ~ 0.07–0.42. Such geometrical analysis is routinely employed for core–shell nanostructures and provides a first-order estimate of the interfacial volume fraction contributing to electronic transport [19]. These values confirm that the system operates in a nanoscale heterojunction regime, where interfacial effects dominate over bulk conduction.

The surface density of fluorine can be estimated from the bulk loading according to:

$$\delta_F = \frac{N_A C_F}{S_{\text{eff}}} \tag{3}$$

where N_A is Avogadro's number and S_{eff} is the effective surface area. For $C_F = 0.20$ mmol g^{-1} and $S_{\text{eff}} = 100$–300 m^2 g^{-1}, this yields ~ 0.4–1.2 F nm^{-2}, which may locally increase to ~ 1–4 F nm^{-2} when accounting for surface roughness and limited accessibility. This range is consistent with reported functional group densities in fluorinated carbon systems and graphene derivatives [20, 21]. Such surface coverages are sufficient to induce measurable work-function shifts in carbon materials due to dipole formation associated with C–F bonds. Fluorination is known to withdraw electron density from the carbon lattice and increase the work function by tens to several hundreds of meV, depending on coverage and bonding configuration [22, 23]. The corresponding modulation of the interfacial barrier height at the Si/SiO_x/C:F junction can be approximated within the classical Schottky–Mott framework:

$$\Delta\phi_B \approx \Delta\phi_{\text{shell}} \tag{4}$$

where $\Delta\phi_{\text{shell}}$ is the fluorination-induced work-function shift of the carbon shell [24]. For partially fluorinated carbon systems, a barrier modulation of $\Delta\phi_B \approx 0.05 - 0.08$ eV is therefore physically reasonable.

Importantly, the sensitivity of nanoscale silicon to such interfacial perturbations is governed

by the Debye length, given by:

$$L_D = \sqrt{\frac{\varepsilon\varepsilon_0 k_B}{k^2 n}} \tag{5}$$

For typical carrier concentrations (10^{17}–$10^{19}\,cm^{-3}$), the Debye length in silicon lies in the range of ~ 1–13 nm, which is comparable to the radius of the nanoparticles used in this study (10–20 nm). Under such conditions (LDR), the entire particle becomes sensitive to surface charge modulation, leading to pronounced conductance changes [25].

Assuming barrier-controlled transport, the electrical resistance follows:

$$R \propto \exp\left(\frac{\varphi_B}{k_B T}\right) \tag{6}$$

and the sensor response can be expressed as:

$$S = \exp\left(\frac{\delta_\varphi}{k_B T}\right) - 1 \tag{7}$$

This exponential dependence implies that even small changes in barrier height (δ_φ ~ 0.02–0.04 eV) can produce multi-fold variations in resistance, consistent with established models of semiconductor gas sensors [25, 26]. Therefore, the experimentally observed 2–2.5-fold enhancement in ammonia response after fluorination can be quantitatively explained by a modest increase in adsorption-induced barrier modulation, driven by fluorination-induced dipoles and work-function shifts in the carbon shell.

NH_3 sensing response and linearity

The gas-sensing performance of the Si@C and Si@C–F hybrids was evaluated at room temperature upon exposure to NH_3 in the concentration range of 1–20 ppm (Fig. 2). The sensor response was defined according to Eq. 7. Upon exposure to NH_3, both materials exhibit an increase in electrical resistance, indicating that adsorption of the reducing gas modulates charge transport across the Si/SiO_x/C heterointerface. However, the magnitude of the response differs significantly between the two systems.

For the fluorinated Si@C–F hybrid, the response increases from ~ 12 r.u. at 1 ppm to ~ 108 r.u. at 20 ppm, demonstrating an approximately linear dependence on ammonia concentration ($S \propto C_{NH_3}$). The high linear regression coefficient ($R^2 > 0.99$) confirms stable and predictable behavior within the low-concentration regime. Notably, the slope of the calibration curve is substantially higher than that of the pristine Si@C sample, indicating enhanced sensitivity following fluorination. In contrast, the non-fluorinated Si@C hybrid exhibits a lower response, ranging from ~ 5 to ~ 43 r.u. over the same concentration interval. Thus, fluorination of the carbon shell results in an approximately 2–2.5-fold increase in sensitivity while preserving linear response characteristics.

Importantly, the preserved linearity suggests that the sensing mechanism in both materials is governed by adsorption-controlled modulation of the interfacial potential barrier, rather than by saturation-limited surface coverage within the investigated concentration range. The sensitivity, defined as the slope $dS/dC(NH_3)$, increases from ~ 2 r.u. $\cdot\, ppm^{-1}$ for Si@C to ~ 5 r.u. $\cdot\, ppm^{-1}$ for Si@C–F, indicating a significant enhancement in charge-transfer modulation efficiency after fluorination.

The improved response of the Si@C–F hybrid correlates with the increased structural disorder and the presence of polar C–F functionalities in the carbon shell, as observed in HRTEM (Fig. 1). Fluorination increases dipole density and modifies the work function of the carbon phase, thereby enhancing band bending at the Si/SiO_x/C interface and amplifying resistance modulation upon NH_3 adsorption.

Dynamic response and humidity effect

Figure 3 presents the dynamic resistance response of the Si@C and Si@C–F hybrid sensors to repeated exposure to 10 ppm NH_3 at room temperature. Three consecutive measurement cycles were conducted under dry argon, followed by an additional cycle at 45% relative humidity (RH, shaded region). Under dry conditions, both mate-

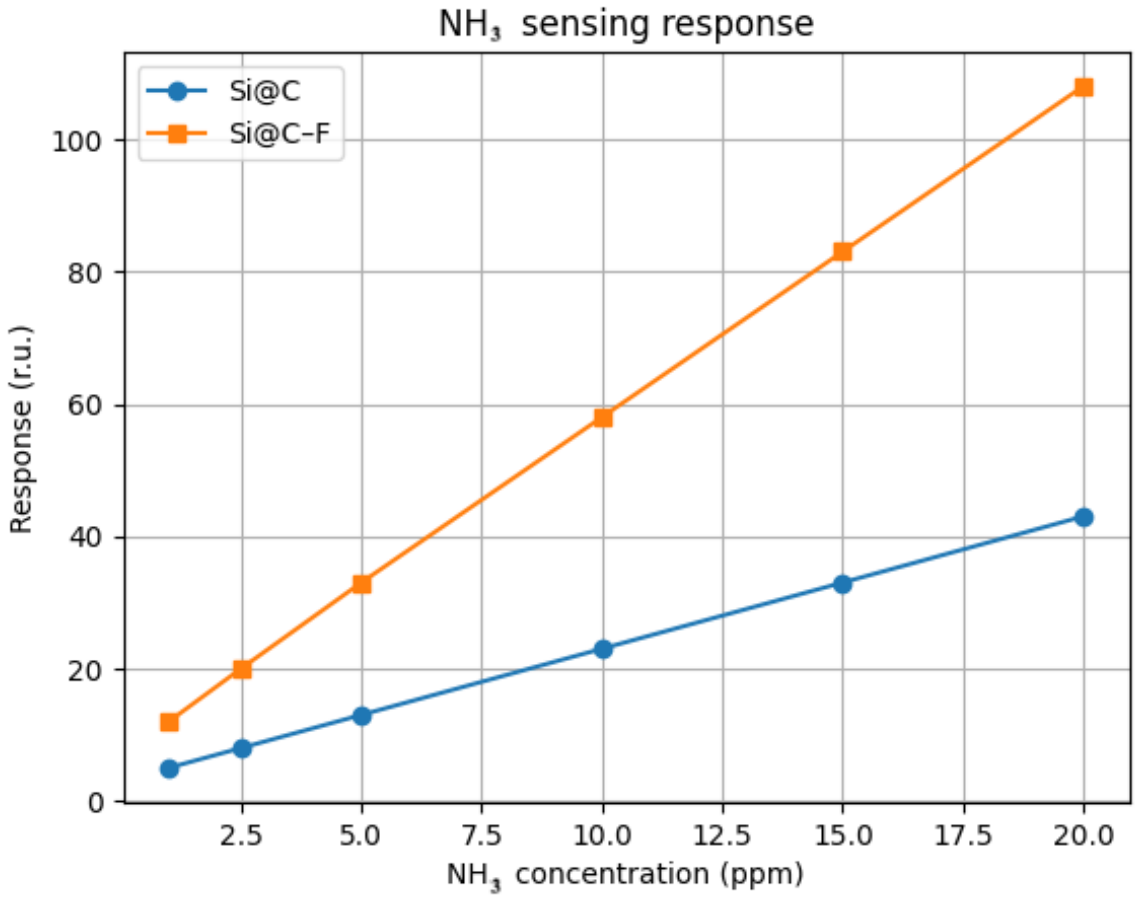

Figure 2 - Comparison of the NH_3 sensing response of the Si@C and Si@C–F hybrids under exposure to ammonia vapor.Measurements performed at room temperature (25 ± 2 °C) under dry argon atmosphere.

rials exhibit stable and reproducible response amplitudes over multiple cycles, indicating good repeatability and the absence of progressive degradation. The Si@C sensor shows response amplitudes in the range of $\sim$ 18–22 r.u., whereas the fluorinated Si@C–F hybrid exhibits significantly higher responses of $\sim$ 50–65 r.u., consistent with the enhanced sensitivity observed in the calibration data (Fig. 2). A slight increase in response amplitude between the first and subsequent cycles likely reflects gradual activation or stabilization of surface adsorption sites rather than irreversible modification, as evidenced by complete baseline recovery after each purge step. The measurements demonstrated good reproducibility across repeated (at least 10) cycles and independently prepared samples, with variation in response amplitude not exceeding ±5–10%. No significant drift or degradation was observed during repeated measurements.

The response kinetics exhibit characteristic adsorption–desorption behavior. Upon NH_3 exposure, the resistance increases monotonically and approaches a quasi-steady state, while purging leads to an exponential-like decay toward the baseline. The response time (t_{90}, defined as the time required to reach 90% of the steady-state value) is approximately 300 s at 10 ppm NH_3, whereas the recovery time is $\sim$ 700 s. The nearly symmetric temporal profiles and reproducible cycling behavior are consistent with a surface-controlled process that can be reasonably described by pseudo-first-order adsorption–desorption kinetics. This observation supports a sensing mechanism governed by reversible modulation of the interfacial potential barrier at the $Si/SiO_x/C$ heterojunction.

Upon increasing the relative humidity to

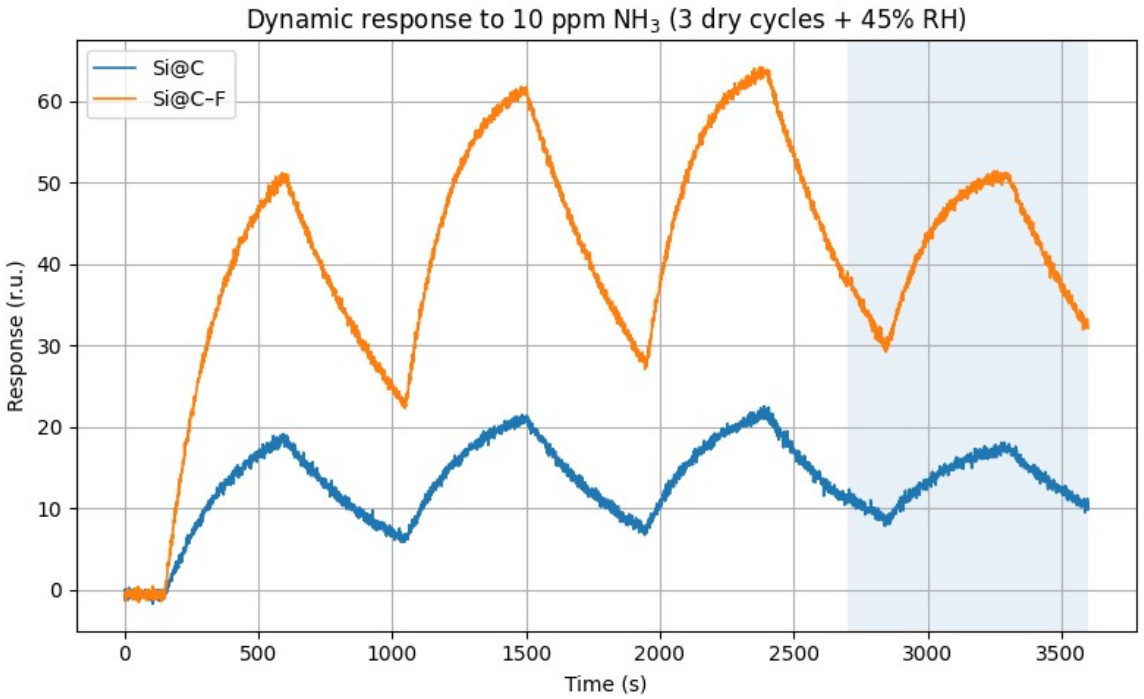

Figure 3 - Dynamic resistance response of Si@C and Si@C–F hybrid sensors at room temperature (25 ± 2 °C) to repeated exposure to 10 ppm NH_3. The first three cycles were measured under dry argon atmosphere, followed by one cycle at 45% RH (shaded region). The fluorinated hybrid exhibits higher response amplitude and excellent repeatability, while humidity induces an increase in baseline resistance and a 20–30% reduction in response magnitude.

45%, two principal effects are observed: (i) Baseline shift. The baseline resistance increases under humid conditions. This behavior can be attributed to competitive adsorption of H_2O molecules, which modify surface dipoles and alter band bending at the Si/SiO_x/C interface. Additionally, water adsorption may influence the effective carrier concentration in the near-surface region of the silicon core through interfacial charge redistribution. (ii) Reduced response amplitude. The NH_3 response decreases by approximately 20–30% for both materials. This reduction is likely caused by partial occupation of active adsorption sites by water molecules and by screening of NH_3-induced dipole interactions at the heterointerface.

To quantify the effect of humidity, a humidity retention factor is defined as:

$$H = \frac{S_{\mathrm{RH}}}{S_{\mathrm{dry}}} \tag{8}$$

where S_{RH} and S_{dry} are the sensor responses under humid and dry conditions, respectively. For the Si@C–F hybrid, H ≈ 0.7–0.8, indicating moderate humidity tolerance typical of carbon-based chemiresistive systems.

Despite partial attenuation, the fluorinated hybrid maintains a substantially higher response amplitude than the pristine Si@C material under both dry and humid conditions. This improved robustness can be attributed to the presence of polar C–F functionalities introduced during fluorination. These groups increase dipole density within the carbon shell and modify its work function, thereby stabilizing interfacial band bending and mitigating complete signal suppression under competitive H_2O adsorption.

Within this framework, NH_3 sensing remains governed by reversible modulation of the interfacial barrier height ($\Delta\phi_{\mathrm{B}}$), rather than irreversible chemical transformation of the sensing layer. The preservation of signal shape, full baseline recovery, and absence of progressive drift under

humid conditions collectively confirm that the sensing mechanism is dominated by reversible, adsorption-induced modulation of the Si/SiO_x/C nanoheterojunction.

Selectivity

Figure 4 compares the response of Si@C and Si@C–F hybrids toward NH_3 (10 ppm) and toward methanol (CH_3OH) and ethanol (C_2H_5OH) vapors at nominal concentrations of $\sim$ 1000 ppm. The dynamic behavior remains cyclic and reversible, similar to that observed for non-fluorinated Si@C hybrids, confirming that fluorination enhances sensitivity without altering the fundamental sensing mechanism. For the fluorinated Si@C–F hybrid, the measured responses are: $S(NH_3,\ 10\ \text{ppm}) \approx 55$ r.u., $S(CH_3OH,\ 1000\ \text{ppm}) \approx 0.2$ r.u., $S(C_2H_5OH,\ 1000\ \text{ppm}) \approx 0.25$ r.u. The corresponding selectivity ratios are therefore: $S(NH_3)/S(CH_3OH) \approx 275$ and $S(NH_3)/S(C_2H_5OH) \approx 220$. Since NH_3 was tested at 10 ppm while alcohol vapors were tested at $\sim$ 1000 ppm, a concentration-normalized selectivity factor provides a more rigorous comparison. The normalized sensitivity (slope-like metric) can be approximated as

$$k = \frac{S}{C_{\text{analyte}}} \tag{9}$$

where S is the signal (in r.u.), and C_{analyte} is the analyte concentration (in ppm). For the Si@C–F hybrid: $k(NH_3) \approx 5.5$ r.u./ppm, $k(CH_3OH) \approx 2 \times 10^{-4}$ r.u./ppm, $k(C_2H_5OH) \approx 2.5 \times 10^{-4}$ r.u./ppm. Thus, the ppm-normalized selectivity factors are $k(NH_3)/k(CH_3OH) \approx 2.8 \times 10^4$ and $k(NH_3)/k(C_2H_5OH) \approx 2.2 \times 10^4$. This indicates that, per unit concentration, NH_3 induces a response approximately four orders of magnitude stronger than alcohol vapors. Such a large selectivity contrast strongly supports a chemically specific sensing mechanism rather than nonspecific adsorption. Notably, the sensor exhibits an orders-of-magnitude higher response to NH_3 at 10 ppm than to alcohol vapors at concentrations 100× higher. This clearly indicates strong chemical selectivity toward ammonia. The weak response to alcohols suggests that the sensing mechanism is not governed by nonspecific adsorption or simple polarity effects, but rather by selective interaction between NH_3 molecules and the interfacial dipole-modulated heterojunction. NH_3, being a strong electron donor with a high dipole moment and lone-pair electrons, more effectively perturbs the interfacial barrier at the Si/SiO_x/C junction than methanol or ethanol. The enhanced selectivity of the Si@C–F hybrid can be rationalized by the presence of polar C–F groups within the carbon shell. Fluorination increases surface polarity and dipole density, strengthening electrostatic interaction with NH_3 molecules and amplifying barrier modulation. At the same time, alcohol adsorption remains weak, likely limited to physisorption without substantial charge transfer. Consistent with previous observations, an increase in baseline resistance with increasing relative humidity (RH) is detected. At 45% RH, the NH_3 response decreases by approximately 15–20%, indicating competitive adsorption of water molecules. Nevertheless, the fluorinated hybrid maintains pronounced selectivity and sensitivity under humid conditions. Importantly, the preserved linear concentration dependence (Fig. 2), stable dynamic behavior (Fig. 3), and strong selectivity (Fig. 4) collectively indicate that fluorination amplifies surface electrostatic coupling without changing the fundamental resistive and surface-controlled nature of charge transport in the hybrid nanostructure.

Role of Molecular Dipole Moment and Donor Strength

The pronounced selectivity toward NH_3 can be rationalized by differences in molecular electronic properties. NH_3 possesses a dipole moment of $\sim$ 1.47 D and features a localized lone pair on nitrogen, making it a strong Lewis base and efficient electron donor. In contrast, methanol ($\mu \approx 1.70$ D) and ethanol ($\mu \approx 1.69$ D) have comparable or slightly higher dipole moments, but their electron density is partially stabilized by O–H bonding and intramolecular interactions, reducing effective charge transfer to the sur-

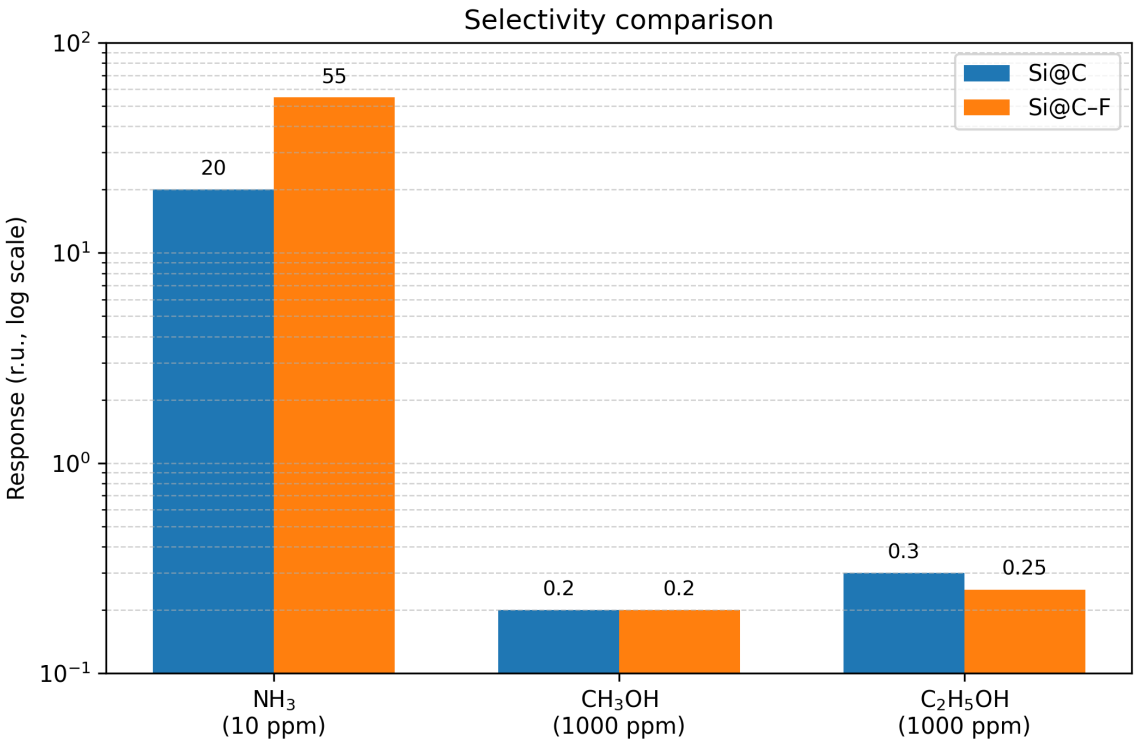

Figure 4 - Selectivity comparison of Si@C and Si@C–F hybrids toward NH_3, CH_3OH, and C_2H_5OH vapors. The response of Si@C–F to methanol and ethanol at nominal concentrations of ~1000 ppm is compared with that to 10 ppm NH_3, demonstrating pronounced selectivity toward ammonia. Measurements performed at room temperature (25 ± 2 °C) under dry argon atmosphere.

face. More importantly, NH_3 can interact directly with electron-deficient surface sites and interfacial dipoles at the Si/SiO_x/C heterojunction, leading to more pronounced modulation of the interfacial barrier height ϕ_B. Alcohol adsorption, in contrast, is likely dominated by weaker hydrogen bonding and physisorption processes, resulting in minimal perturbation of the interfacial potential.

In the fluorinated Si@C–F hybrid, the presence of polar C–F groups increases local electrostatic fields and dipole density within the carbon shell. This enhances sensitivity to molecules capable of strong donor–acceptor interactions, such as NH_3, while not significantly amplifying response to weakly interacting alcohol vapors. Therefore, fluorination selectively strengthens electrostatic coupling rather than indiscriminately increasing surface adsorption.

Mechanistic considerations

Fluorination of the carbon shell modifies the interfacial electronic structure of the Si/SiO_x/C nanoheterojunction. Due to the strong electron-withdrawing character of fluorine ($\chi_F = 3.98$), the introduction of C–F dipoles increases the effective work function of the carbon shell ($W_{C:F} > W_C$). This results in enhanced band bending and an increased built-in potential at the Si/SiO_x/C:F interface. The heterostructure can be approximated as a Schottky-like nanojunction in which electrical transport is governed by thermally activated barrier-controlled conduction rather than bulk silicon conductivity. In this framework, the resistance therefore follows

$$R \propto\propto \exp\left(\frac{q\varphi_B}{k_B T}\right) \qquad (10)$$

where q is the elementary charge (1.6×10^{-19} C), k_B is the Boltzmann constant, T is the absolute temperature, and ϕ_B is the effective interfa-

cial barrier height.

Upon adsorption of electron-donating NH_3 molecules, the interfacial dipole field is partially compensated, resulting in a reduction of the barrier height

$$\Delta\phi_{B,gas} = \phi_{B,0} - \Delta\phi_{ads} \tag{11}$$

where ϕ_B, 0 is the initial barrier height in air (or carrier gas), and $\Delta\phi_{ads}$ is the adsorption-induced barrier reduction.

Because transport depends exponentially on ϕ_B, even moderate barrier modulation ($\Delta\phi_B \approx$ 0.05–0.08) can produce multi-fold amplification of the electrical response at room temperature. For small perturbations, the relative resistance change may be approximated as ($\Delta\phi_B \ll k_B T/q$), the relative resistance change can be approximated as:

$$\frac{\Delta R}{R_0} \approx \frac{q}{k_B T}\Delta\phi_B \tag{12}$$

highlighting the high sensitivity of barrier-controlled transport to interfacial potential variations.

Given that the silicon nanoparticles have diameters of 20–40 nm, which may be comparable to the Debye screening length in moderately doped silicon - the depletion region can extend over a significant fraction of the nanoparticle volume. In this quasi-full-depletion regime, small variations in surface potential effectively modulate the entire conductive pathway. Fluorination therefore transforms the Si@C interface into a more electrostatically sensitive nanojunction characterized by increased work-function contrast, stronger interfacial dipole fields, and enhanced barrier modulation under NH_3 adsorption. The experimentally observed increase in baseline resistance, higher sensitivity, and preserved linearity are fully consistent with this interfacial electronic-structure model. Direct experimental verification of the work-function shift (e.g., Kelvin probe or UPS) is beyond the scope of this study but represents an important direction for future work.

CONCLUSIONS

Si@C hybrid nanostructures with particle sizes of 20–40 nm demonstrate efficient room-temperature ammonia sensing, characterized by linear response in the 1–20 ppm range and pronounced selectivity over alcohol vapors. The sensing behavior is governed by interfacial charge transfer at the Si/SiO_x/C heterojunction, where the depletion region extends over a significant fraction of the nanoparticle volume, enabling strong sensitivity to surface potential variations. Fluorination of the carbon shell enhances performance by increasing surface polarity and work function, thereby strengthening interfacial dipole fields and amplifying barrier modulation under NH_3 adsorption. This results in a substantial increase in sensitivity while preserving linearity and reversibility. These findings highlight fluorination as an effective strategy for tuning interfacial electronic structure in Si–C nanohybrids and establish barrier-controlled transport at nanoscale heterojunctions as a key mechanism for high-performance room-temperature gas sensing. The key contribution of this work is the demonstration that fluorination-induced dipole fields and work-function modification in the carbon shell can effectively control interfacial barrier properties in Si/SiO_x/C nanoheterojunctions. This provides a simple and scalable strategy for tuning sensitivity and selectivity of semiconductor gas sensors operating at room temperature.

ACKNOWLEDGMENT

This research was funded by the Committee of Science of the Ministry of Science and Higher Education of the Republic of Kazakhstan (grant no. AP22683909).

Author Contributions: D. Ye.: Investigation, Writing–Original Draft, Funding Acquisition; S. B.: Investigation, Writing–Review and Editing; G. Y–M.: Writing–Review and Editing; O. Yu. B.: Investigation, Writing–Review and Editing; V. L.: Writing and Editing, Supervision; V. V. L.: Writing–Review and Editing, Conceptualization, Supervision; G. M.: Conceptualization, Writing–Original Draft, Writing–Review and Editing, Supervision.

REFERENCES

[1] Yamazoe, N. and K. Shimanoe. "Theory of power laws for semiconductor gas sensors." *Sensors and Actuators B: Chemical* 128, no. 2 (2008): 566–573.

[2] Korotcenkov, G. "Metal oxides for solid-state gas sensors: What determines our choice?" *Materials Science and Engineering* 139, no. 1 (2007): 1–23.

[3] Barillaro, G. "Porous silicon gas sensing."*In* , edited by L. Canham, 845–856. Cham: Springer, 2014.

[4] Schedin, F., A. K. Geim, S. V. Morozov, E. W. Hill, P. Blake, M. I. Katsnelson, and K. S. Novoselov. "Detection of individual gas molecules adsorbed on graphene." *Nature Materials* 6, no. 9 (2007): 652–655.

[5] Nakysbekov, Z., B. Zhumadilov, B. Medyanova, G. Partizan, G. Suyundykova, and B. Aliev. "Synthesis of two-dimensional nanostructures at low temperatures." *International Journal of Mathematics and Physics* 16, no. 1 (2025): 41–46.

[6] Gritsenko, L., Z. Kalkozova, Y. Kedruk, Z. Paltusheva, M. Mussakhanov, and K. Abdullin. "$Znco_2o_4$ nanostructure-based electrochemical sensor for highly sensitive glucose detection." *Physical Sciences and Technology* 12, no. 3–4 (2025): 50–59.

[7] Kong, J., N. Franklin, C. Zhou, M. Chapline, S. Peng, K. Cho, and D. H. "Nanotube molecular wires as chemical sensors." *Science* 287, no. 5453 (2000): 622–625.

[8] Linevych, Y., V. Koval, M. Dusheiko, M. Lakyda, N. Kavraska, V. Barbash, and T. P. "Carbon surface modification of silicon nanowires for sensing application." *Sensors and Actuators A: Physical* 389 (2025): 116534.

[9] Mussabek, G., N. Zhylkybayeva, S. Baktygerey, D. Yermukhamed, Y. Taurbayev, G. Sadykov, A. Zaderko, and V. Lisnyak. "Preparation and characterization of hybrid nanopowder based on nanosilicon decorated with carbon nanostructures." *Applied Nanoscience* 13 (2023): 6709–6718.

[10] Kashaykin, P. F., E. A. Pospelova, I. Kenzhina, Z. A. Zaurbekova, S. K. Askerbekov, M. Y. Salgansky, A. A. Shaimerdenov, A. U. Tolenova, and A. L. Tomashuk. "Gamma-radiation-induced attenuation of light in pure-silica core optical fiber in long-wavelength region." *International Journal of Mathematics and Physics* 13, no. 1 (2000): 75–81.

[11] Robinson, J. T., J. S. Burgess, C. E. Junkermeier, S. C. Badescu, T. L. Reinecke, F. K. Perkins, M. K. Zalalutdniov, J. W. Baldwin, J. C. Culbertson, P. E. Sheehan, and E. S. Snow. "Properties of fluorinated graphene films." *Nano Letters* 10, no. 8 (2010): 3001–3005.

[12] Withers, M., F.and Dubois and A. K. Savchenko. "Electron properties of fluorinated single-layer graphene transistors." *Physical Review* 82, no. 7 (2010): 073403.

[13] Kim, H. J. and J. H. Lee. "Highly sensitive and selective gas sensors using p-type oxide semiconductors: Overview." *Sensors and Actuators B: Chemical* 192 (2014): 607–627.

[14] Tang, X., M. Debliquy, D. Lahem, Y. Yan, and J.-P. Raskin. "A review on functionalized graphene sensors for detection of ammonia." *Sensors* 21 (2021): 1443.

[15] Li, T., H. Duan, L. Daukiya, L. Simon, and K. Leifer. "Enhanced ammonia gas adsorption through site-selective fluorination of graphene." *Crystals* 12, no. 8 (2022): 1117.

[16] Lisnyak, V., G. Mussabek, N. Zhylkybayeva, S. Baktygerey, and A. Zaderko. "Preparation and characterization of carbon-silicon hybrid nanostructures." *Journal of Nano- and Electronic Physics* 13, no. 5 (2021): 05035.

[17] Mussabek, G., S. Baktygerey, Y. Taurbayev, D. Yermukhamed, N. Zhylkybayeva, A. Zaderko, V. Diyuk, S. Afonin, G. Yar-Mukhamedova, R. Mariychuk, L. Grishchenko, M. Kaňuchová, and V. Lisnyak. "Surface chemistry and catalytic activity in h2o2 decomposition of pyrolytically fluoralkylated activated carbons." *RSC Advances* 14, no. 40 (2024): 29 052–29 071.

[18] Diyuk, V., A. Zaderko, L. Grishchenko, S. Afonin, R. Mariychuk, O. Boldyrieva, V. Skryshevsky, M. Kaňuchová, and V. Lisnyak. "Surface chemistry of fluoroalkylated nanoporous activated carbons: Xps and 19f nmr study." *Applied Nanoscience* 12, no. 3 (2022): 637–650.

[19] Caruso, F. "Nanoengineering of particle surfaces." *Advanced Materials* 13 (2001): 11–22.

[20] Dreyer, D. *et al.* "The chemistry of graphene oxide." *Chemical Society Reviews* 39 (2010): 228–240.

[21] Liu, Y., L. Jiang, H. Wang, H. Wang, W. Jiao, G. Chen, P. Zhang, D. Hui, and X. Jian. "A brief review for fluorinated carbon: Synthesis, properties and applications." *Nanotechnology Reviews* 8 (2019): 573–586.

[22] Nair, R. *et al.* "Fluorographene: A two-dimensional counterpart of teflon." *Small* 6 (2010): 2877–2884.

[23] Withers, F., M. Dubois, and A. Savchenko. "Electron properties of fluorinated single-layer graphene transistors." *Physical Review B* 82 (2010): 073403.

[24] Yamazoe, N. "New approaches for improving semiconductor gas sensors." *Sensors and Actuators B* 5 (1991): 7–19.

[25] Barsan, N. and U. Weimar. "Conduction model of metal oxide gas sensors." *Journal of Electroceramics* 7 (2001): 143–167.

[26] Yamazoe, N. and K. Shimanoe. "Theory of power laws for semiconductor gas sensors." *Sensors and Actuators B* 128 (2008): 566–573.

Information about authors

Dana Yermukhamed *– PhD, Senior Researcher at Institute of Information and Computational Technologies, Almaty, Kazakhstan. Assistant professor at the Department of Solid-State Physics and New Materials Technology at Al-Farabi Kazakh National University, Almaty, Kazakhstan, email: danayermukhamed92@gmail.com*

Saule Z. Baktygerey *– MS in Nanomaterials and nanotechnologies, Junior Researcher at Nanotechnological Laboratory of Open at Al-Farabi Kazakh National University, Almaty, Kazakhstan, email: bs.saule18@gmail.com*

Gulmira Sh. Yar-Mukhamedova *– Dr.of Physical and Mathematical Sciences, Professor, Professor-Researcher at the Department of Solid State Physics and Technology of New Materials at Al-Farabi Kazakh National University, Almaty, Kazakhstan, email: shariphovna@gmail.com*

Alimzhan M. Serikbekov *– MS in Nanomaterials and nanotechnologies, PhD student at Al-Farabi Kazakh National University, Almaty, Kazakhstan, email: alimzhan.serikbekov2002@gmail.com*

Olga. Yu. Boldyrieva *– PhD, Assoociate Professor at the Chemical Faculty, Kyiv National Taras Shevchenko University, Kyiv,Ukraine, email: ob@univ.kiev.ua;*

Vladimir Lysenko *– PhD, Senior Researcher, Institute of Light and Matter Lyon, Villeurbanne, France. email: vladimir.lysenko@univ-lyon1.fr*

Vladyslav V. Lisnyak *– Dr.of Chemical Sciences, Professor, Senior Researcher at the Institute of Surface Chemistry, NAS of Ukraine, Kyiv, Ukraine, email: lisnyak@nas.gov.ua*

Gauhar K. Mussabek *– PhD, Associate Professor, Research Professor at the Department of Solid-State Physics and New Materials Technology at Al-Farabi Kazakh National University, Almaty, Kazakhstan. Leading Researcher at Institute of Information and Computational Technologies, Almaty, Kazakhstan, email: gauhar.musabek@kaznu.edu.kz*